Anusandhanvallari
Vol 2024, No.1
July 2024
ISSN 2229-3388

Classical versus Quantum Vibrational Spectra of Isolated and Coupled Morse Oscillators

Rupashi Bhardwaj* Sonu Ram Shankar*[1]

*University Department of Chemistry, Lalit Narayan Mithila University, Darbhanga, Bihar, India. 846004.

Abstract: Classical molecular dynamics provides a computationally economical approach to finite-temperature vibrational spectroscopy; but, its reliability is limited by the absence of vibrational quantization, zero-point energy, and discrete quantum state mixing. This study examines the validity of the classical description by direct comparisons with quantum calculations for controlled anharmonic model systems. Isolated Morse oscillators with nominal frequencies of 300 and 3800 cm^{-1} were investigated using linear, quadratic, and cubic dipole moment functions to distinguish the effects of mechanical and electrical anharmonicities. A two-dimensional system of coupled Morse oscillators with frequencies of 1900 and 3800 cm^{-1} was subsequently employed to examine the temperature dependence and the Fermi resonance. Identical potential energy and dipole moment functions were used in classical and quantum calculations. Classical molecular dynamics reproduced the principal band and overall spectral profile of the low-frequency oscillators. However, for the high-frequency oscillator, the classical fundamental was blue-shifted relative to the quantum transition, and the disagreement increased substantially for the higher-order spectral features. The nonlinear dipole functions generated overtone-like features in both descriptions, although their positions and relative intensities showed an increasing classical–quantum divergence. Increasing the temperature produced greater fragmentation of the classical spectra through sampling of more anharmonic regions of the potential energy surface, whereas the quantum transition frequencies remained comparatively stable. Both approaches qualitatively reproduced the coupling-induced splitting associated with the Fermi resonance; however, the strong coupling generated considerably greater spectral congestion in classical results. Classical molecular dynamics is therefore the most reliable method for low-frequency motion, qualitative trends, and overall spectral envelopes, whereas quantum treatment remains necessary for high-frequency stretching vibrations, higher-order transitions, and detailed resonance assignments.

Keywords: Vibrational spectroscopy; Morse oscillator; mechanical anharmonicity; electrical anharmonicity; Fermi resonance; vibrational coupling

1. Introduction

Vibrational spectroscopy establishes a direct connection between molecular structure and nuclear motion, making infrared and Raman techniques indispensable for identifying chemical species, determining bond strengths and molecular geometries, and investigating conformational changes, intermolecular interactions, and chemical transformations [1–5]. Within the Born–Oppenheimer approximation, electronic and nuclear motions are separated, and nuclear vibrational motion is described on the potential energy surface associated with a particular electronic state, usually the ground electronic state. [6]. A nonlinear molecule containing Natoms has 3N-6 normal vibrational modes, whereas a linear molecule has 3N-5. Near equilibrium, each mode is typically represented as an independent, harmonic oscillator with $V(q) = \frac{1}{2}kq^2$and $E_v = \left(v + \frac{1}{2}\right)h\nu$. Although this approximation is useful for assigning fundamental frequencies, it predicts equally spaced energy levels and the selection rule $\Delta v = \pm 1$; therefore, it cannot describe dissociation, overtones, combination bands, excitation-dependent frequency shifts, or strong interactions between vibrational modes [1–3]. The real molecular potentials are also anharmonic. For bond stretching, the Morse potential, $V(r) = D_e[1 - \exp\{-a(r - r_e)\}]^2$, provides a physically meaningful model because it is asymmetric, approaches a finite dissociation limit, and produces progressively decreasing vibrational level spacings. [7]. Anharmonicity may be mechanical, arising from higher-order terms in the potential

energy surface, or electrical, resulting from the nonlinear dependence of the molecular dipole moment or polarizability on nuclear displacement. Both forms affect the spectral frequency and intensity. Accurate quantum-mechanical treatments include the vibrational self-consistent field, vibrational configuration interaction, perturbative multiconfiguration time-dependent Hartree, and variational nuclear motion methods. [10–15]. These approaches can provide highly accurate vibrational energies and transition intensities; however, their computational cost increases rapidly with the molecular size, number of coupled vibrational modes, and dimensionality required to represent the potential energy and dipole moment surfaces or dipole moments. Consequently, contemporary methods seek reduced-dimensional representations, automated perturbative treatments, and mode-tailored potential surfaces that retain important anharmonic couplings while avoiding the construction of a complete multidimensional surface [19,21,26]. Classical molecular dynamics provides a computationally economical alternative for studying large molecules, liquids, clusters, and condensed phases. Nuclear trajectories are generated from Newton's equations, $m_i\ddot{r}_i = -\nabla_i V(r)$, and the infrared spectrum can be evaluated from the Fourier transform of a dipole or dipole-velocity autocorrelation function, $\alpha(\omega) \propto \beta\omega^2 \int_{-\infty}^{\infty} \langle \mu(0) \cdot \mu(t) \rangle e^{-i\omega t} dt$, apart from conventional prefactors [4,9,16,17]. Because trajectories explore an anharmonic potential at finite temperatures, molecular dynamics naturally incorporates thermal fluctuations, conformational sampling, environmental interactions, and spectral broadening. It can be combined with empirical force fields, density functional theory, ab initio electronic structure calculations, or machine-learned potential energy surfaces [16,20,25,27,28]. Nevertheless, ordinary classical trajectories do not contain discrete vibrational energy levels, zero-point energy, tunnelling, quantum coherence, or exact quantum selection rules. Classical simulations are therefore expected to be most reliable for relatively low-frequency modes and thermally accessible motions, whereas significant deviations may arise for high-frequency stretching vibrations, low temperatures, overtone transitions, proton transfer coordinates, and strongly coupled modes. [18,19,21]. Recent developments have attempted to bridge the classical–quantum divide using path integral simulations, Wigner-sampled molecular dynamics, constrained nuclear–electronic orbital methods, and semiclassical trajectory formulations. [22–24,29]. These approaches have demonstrated that nuclear quantum effects can substantially influence the positions, widths, intensities, and coupling patterns of vibrational bands, particularly in water, hydrogen-bonded systems, and highly anharmonic proton-transfer coordinates. [18,23,24,27,28]. Vibrational coupling is an especially stringent test. Fermi resonance occurs when vibrational states of the same symmetry—commonly a fundamental overtone or combination state—are nearly degenerate and coupled through anharmonic terms. Their interaction produces avoided crossings, level splitting, and redistribution of spectral intensity, including intensity borrowing by an otherwise weak transition [8,19,21]. Recent combined theoretical and experimental studies have demonstrated that such resonances remain important in organic hydrates and other hydrogen-bonded complexes, where nuclear quantum effects and intermolecular coupling can complicate seemingly simple stretching bands. [28,30]. Temperature also affects the classical and quantum descriptions differently: in classical molecular dynamics, it modifies the amplitudes and regions of the potential surface sampled by trajectories, whereas quantum mechanically, it primarily changes the Boltzmann populations of the discrete states. Therefore, the present study employed controlled model systems to determine the domain of validity of classical molecular dynamics for vibrational spectroscopy. An isolated Morse oscillator was used to compare the low- and high-frequency motions and separate the mechanical anharmonicity from the electrical anharmonicity introduced through the nonlinear dipole functions. A two-dimensional system of coupled Morse oscillators was subsequently used to examine the onset and evolution of the Fermi resonance as the coupling strength and temperature were varied. A direct comparison with quantum calculations under identical model conditions allows the differences in peak positions, intensities, overtone features, thermal responses, and coupling-induced splitting to be attributed specifically to the classical treatment of nuclear motion. The objective of this study is to establish when classical molecular dynamics provides a reliable representation of an anharmonic vibrational spectrum and when an explicit quantum-mechanical or quantum-corrected treatment becomes indispensable.

2. Computational Methodology

2.1. Model Systems

Two model systems were used to compare classical molecular dynamics (MD) with quantum-mechanical calculations. The first was a one-dimensional Morse oscillator described as $V(q) = D_e\left[1 - e^{-a(q-q_e)}\right]^2$, which incorporates anharmonicity and finite dissociation energy. Low- and high-frequency oscillators are represented by $(\omega_e, \omega_e x_e) = (300, 15)$ and $(3800, 150)$ cm^{-1}, respectively, and are generally studied at 150 K.

The second system comprised two coupled Morse oscillators with frequencies of 3800 and 1900 cm^{-1}. Because the overtone of the lower-frequency mode is close to the fundamental frequency of the higher-frequency mode, the system exhibits a Fermi resonance. The coupling parameters COUP0 $= 0$, COUP1 $= 1.0 \times 10^{-3}$, and COUP2 $= 1.5 \times 10^{-1}$ represent the uncoupled, weakly coupled, and strongly coupled conditions, respectively. Calculations for this system were performed at 300 K.

2.2. Dipole Moment Models

Electrical anharmonicity was examined using dipole functions proportional to q, q^2, and q^3:

$$\mu_n(q) \propto q^n,\ n = 1,2,3.$$

These linear, quadratic, and cubic models allow higher-order spectral features to acquire intensity without changing the Morse potential, thereby separating the electrical and mechanical anharmonicity. For the coupled system, the total dipole moment is expressed as $\mu = x + y$,

where and are the two vibrational coordinates. Identical dipole functions were used for the classical and quantum calculations.

2.3. Classical Molecular Dynamics Simulations

Classical trajectories were generated using Newton's equation as follows:

$$m_i \frac{d^2 r_i}{dt^2} = -\nabla_i V(r)$$

Each system was equilibrated at the selected temperature using a canonical NVT trajectory. Thirty independent microcanonical NVE trajectories were then initiated from the equilibrated configurations, allowing the vibrational motion to evolve without any interference from the thermostat.

The time-dependent dipole moments were recorded for each trajectory. The infrared spectrum was obtained from the Fourier transform of the autocorrelation function as follows:

$$I_{MD}(\omega) \propto \omega \int_{-\infty}^{\infty} \langle \mu(0) \cdot \mu(t) \rangle\, e^{-i\omega t}\, dt$$

The spectra of the 30 trajectories were averaged to reduce statistical fluctuations. The temperature effects were examined by varying the NVT equilibration temperature while retaining the same production and analysis procedures.

2.4. Quantum Dynamical Calculations

Reference spectra were obtained by solving the vibrational Schrödinger equation:

$$\hat{H}\Psi_v = E_v \Psi_v.$$

Transition intensities were calculated from

$$I_{ij} \propto |\langle \Psi_i | \hat{\mu} | \Psi_j \rangle|^2.$$

Thus, quantum calculations produce discrete vibrational energies and transition intensities, whereas classical MD generates continuous trajectory. Identical potentials, dipole functions, temperatures, and coupling parameters were employed wherever applicable.

2.5. Spectral Comparison

The classical and quantum spectra were compared in terms of peak positions, relative intensities, spectral envelopes, higher-order features, temperature dependence, and coupling-induced splitting. This comparison isolates the effects of vibrational frequency, mechanical and electrical anharmonicity, temperature, and Fermi coupling on the validity of classical MD simulations for vibrational spectroscopy.

Table 1. Computational Models and Simulation Parameters Used in the Present Study.

Category	Parameter	Morse Oscillator	Fermi Resonance Model	Remarks
Potential Model	Potential energy function	Morse	Two coupled Morse oscillators	Anharmonic PES
	Number of dimensions	1	2	Single vs coupled modes
Vibrational Parameters	Fundamental frequency	300 or 3800 cm^{-1}	3800 & 1900 cm^{-1}	Low- and high-frequency models
	Anharmonicity constant	15 or 150 cm^{-1}	Model dependent	Source-derived values
	Coupling strength	—	COUP0, COUP1, COUP2	Three interaction regimes
Dipole Model	Dipole function	Linear, quadratic, cubic	$\mu = x + y$	Electrical anharmonicity
Simulation Conditions	Temperature	150 K	300 K	Unless otherwise stated
	Equilibration	1 NVT trajectory	1 NVT trajectory	Canonical ensemble
	Production runs	30 NVE trajectories	30 NVE trajectories	Ensemble averaging
Spectral Calculation	Spectral method	Fourier transform	Fourier transform	Time-domain → frequency-domain
	Final spectrum	Average of 30 spectra	Average of 30 spectra	Statistical improvement
Reference Method	Quantum calculation	Vibrational Schrödinger equation	Vibrational Schrödinger equation	Benchmark calculations

3. Results and Discussion

This comparison was designed to determine the conditions under which classical molecular dynamics (MD) can reproduce quantum vibrational spectra and identify the origins of the deviations between the two descriptions. The analysis progresses from an isolated Morse oscillator to models that incorporate nonlinear dipole functions, temperature variations and Fermi coupling. Because identical potential energy and dipole moment functions were used in the classical and quantum calculations, the observed differences primarily arise from their different treatments of nuclear motion. The results were evaluated at three levels: the reproduction of the principal spectral pattern, accuracy of individual peak positions and intensities, and interpretation of higher-order or coupling-induced features.

3.1. Frequency Dependence of Classical–Quantum Agreement

The isolated Morse oscillator provides the clearest test of the classical approximation because it contains mechanical anharmonicity without additional complications from mode coupling. Figure 4.1 compares the classical and quantum spectra calculated using a linear dipole function at 150 K for oscillators with nominal frequencies of 300 and 3800 cm^{-1}.

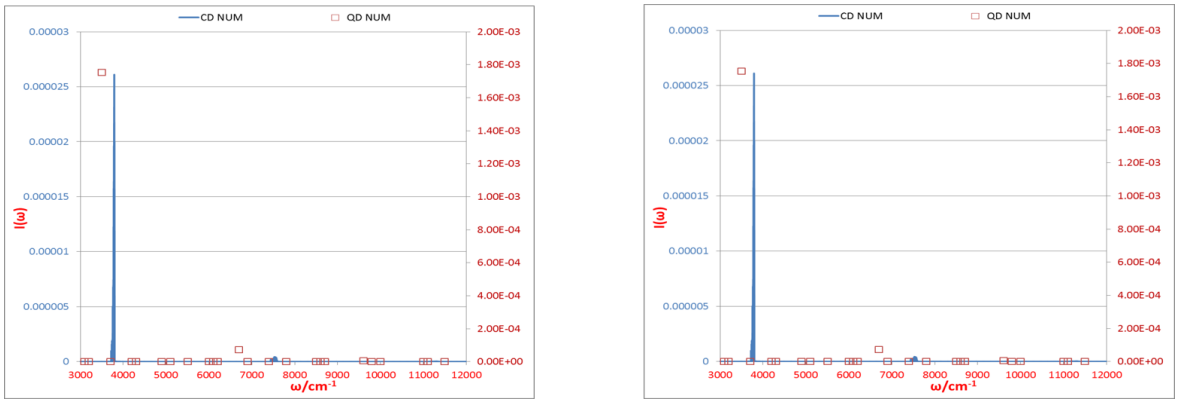

Figure 1. Classical and quantum vibrational spectra of isolated Morse oscillators with a linear dipole function, , at 150 K: (a) low-frequency oscillator with nominal frequency 300 cm^{-1} and (b) high-frequency oscillator with nominal frequency 3800 cm^{-1}.

Solid curves represent spectra obtained from classical molecular dynamics, while open squares indicate discrete quantum transitions. Classical and quantum intensities are displayed against the left and right ordinates, respectively; consequently, the comparison concerns peak positions and spectral patterns rather than absolute intensity magnitudes.

Table 2. Comparison of Principal Spectral Features for the Linear Dipole Model.

Quantity	**300 cm^{-1} Oscillator**	**3800 cm^{-1} Oscillator**
QD fundamental peak (cm^{-1})	285	**3558**
MD fundamental peak (cm^{-1})	295	**3776**
Peak shift (cm^{-1})	10	**218**
Relative error (%)	3.5	6.1
Agreement	Excellent	Moderate
Higher-frequency features	Weak	Very weak

For the 300 cm^{-1} oscillator, the principal quantum transition occurs near 280 cm^{-1}, whereas the classical maximum lies near 295 cm^{-1}. This difference of 15 cm^{-1} corresponds to a relative deviation of 5%. Thus, classical MD reproduces the position and overall profile of the dominant, low-frequency band. Nevertheless, its spectrum is broader and contains weak features around 500–600 cm^{-1}. They may arise from higher-order anharmonic motion, finite trajectory effects, or the details of the spectral transformation.

For the 3800 cm^{-1} oscillator, the quantum transition occurred at 3558 cm^{-1}, whereas the classical maximum was found at 3776 cm^{-1}. Therefore, the classical blue shift is $\Delta\tilde{\nu} = 3776 - 3558 = 218\ cm^{-1}$, corresponding to a relative deviation of $\approx 6.1\%$. Although the percentage deviations for the low- and high-frequency fundamentals appear numerically comparable, the absolute displacement increases from 15 to 218 cm^{-1}. Moreover, the high-frequency classical peak remains close to the nominal harmonic frequency, whereas anharmonic quantization shifts the quantum transition substantially towards lower frequencies. This difference becomes more pronounced for higher-order features, as discussed in the following sections.

The quantum Morse oscillator possesses discrete, progressively compressed vibrational levels, whereas classical trajectories are not restricted to discrete eigenstates and do not exhibit zero point motion. Consequently, the classical description becomes increasingly inadequate as the vibrational energy spacing and quantum characteristics of motion increase. The values are presented in Table 2.

These findings demonstrate that mechanical anharmonicity alone does not determine the validity of classical MD simulation results. The vibrational frequency is equally important: low-frequency motion approaches the classical regime, whereas high-frequency stretching exhibits a pronounced quantum character.

3.2. Influence of Electrical Anharmonicity

Electrical anharmonicity arises when the molecular dipole moment varies nonlinearly with vibrational displacement. Unlike mechanical anharmonicity, which modifies the energy levels through the potential-energy function, electrical anharmonicity changes the transition intensities and allows higher-order spectral features to acquire intensities. Figure 2 compares the spectra generated using linear, quadratic, and cubic dipole functions while retaining the same Morse potential and temperature.

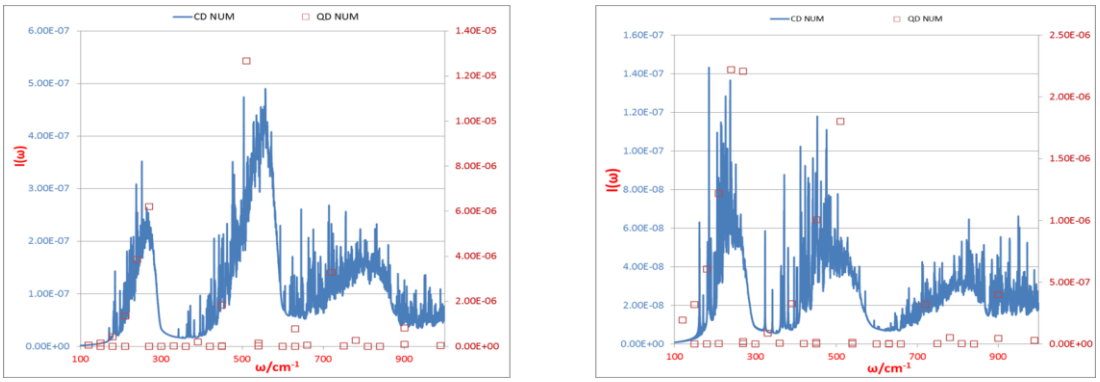

Figure 2. Influence of electrical anharmonicity on the vibrational spectrum of the 300 cm^{-1} Morse oscillator at 150 K: (a) quadratic dipole function and (b) cubic dipole function .

Solid curves show classical molecular-dynamics spectra, and open squares show quantum transition intensities. Nonlinear dipole functions generate higher-order spectral features in both descriptions, although the classical bands are broader and do not reproduce every discrete quantum transition.

For the 300 cm^{-1} oscillator, the quadratic and cubic models produced multi-band spectra in both descriptions. The quantum spectra contain prominent features near 270, 510, and 720–730 cm^{-1}, whereas the quadratic-dipole classical spectrum has maxima near 280, 550, and 800 cm^{-1}. The cubic model yielded a comparable distribution, although its intermediate region was broader and less resolved. Classical MD, therefore, reproduces the general low-frequency spectral envelope but not a precise one-to-one correspondence between individual discrete transitions. The broader classical bands reflect the continuous distribution of oscillatory frequencies sampled by the ensemble of trajectories.

The disagreement is substantially greater for the 3800 cm^{-1} oscillators. The quadratic and cubic classical spectra contain features near 3780, 7550–7600, and 11,200 cm^{-1}, whereas the corresponding quantum features are near 3560, 6800–6900, and 9600 cm^{-1}. Therefore, the classical blue shifts are $\Delta\tilde{\nu}_1 \approx 220$, $\Delta\tilde{\nu}_2 \approx 700$, $\Delta\tilde{\nu}_3 \approx 1600$ cm^{-1}.

These values, summarized in Table 3, show that the divergence increases rapidly with increasing spectral order.

Table 3. Spectral features obtained using the nonlinear dipole functions.

Dipole function	**Oscillator frequency** / cm^{-1}	**Quantum features** / cm^{-1}	**Classical features** / cm^{-1}	**Main observation**

Squared	300	270, 510, 730	280, 550, 800	General multi-band profile reproduced
Cubic	300	270, 510, 720–730	280, broad intermediate band, 780–820	Similar overall envelope, but greater broadening
Squared	3800	3560, 6800–6900, 9600	3780, 7550–7600, 11,200	Increasing classical blue shift
Cubic	3800	3560, 6800–6900, 9600	3780, 7550–7600, 11,200	Similar trend with stronger higher-order disagreement

This trend follows from the different energy structures of the two descriptions. Nonlinear classical dipole functions generate components related to multiples and combinations of the underlying continuous oscillatory motions. However, in a quantum Morse oscillator, the energy levels become progressively closer as the excitation increases. Therefore, higher transitions do not remain as exact multiples of the fundamental frequency. The classical spectrum remains closer to the harmonic progression and consequently exhibits increasingly large blue shifts relative to the quantum transitions.

The nonlinear dipole functions also redistribute the spectral intensities. Both descriptions predict the appearance or enhancement of higher-order features, showing that classical MD captures the qualitative effects of anharmonicity. However, the relative intensities and positions of these features are increasingly sensitive to quantization, particularly in the case of high-frequency oscillators. Therefore, agreement in the fundamental band alone should not be considered a sufficient validation of the classical calculation. The peak positions, relative intensities, and progression of the higher-order features must be examined collectively.

3.3. Temperature Dependence of Classical and Quantum Spectra

Figure 4.3 compares the temperature-dependent spectra of the coupled Morse system for a fixed coupling strength. The two theoretical descriptions respond differently to temperature increases. The quantum spectra show little change in their principal transition frequencies and only limited redistribution of intensity over the investigated temperature range. The vibrational energies remain fixed by the eigenvalues of the Hamiltonian, whereas the temperature changes the Boltzmann populations as follows:

$$P_v = \frac{e^{-E_v/k_B T}}{Z}$$

where P_v is the population of the state, and Z is the vibrational partition function. Under the conditions studied, the higher states of the high-frequency oscillator remain only weakly populated; consequently, the dominant quantum features remain relatively stable.

Anusandhanvallari
Vol 2024, No.1
July 2024
ISSN 2229-3388

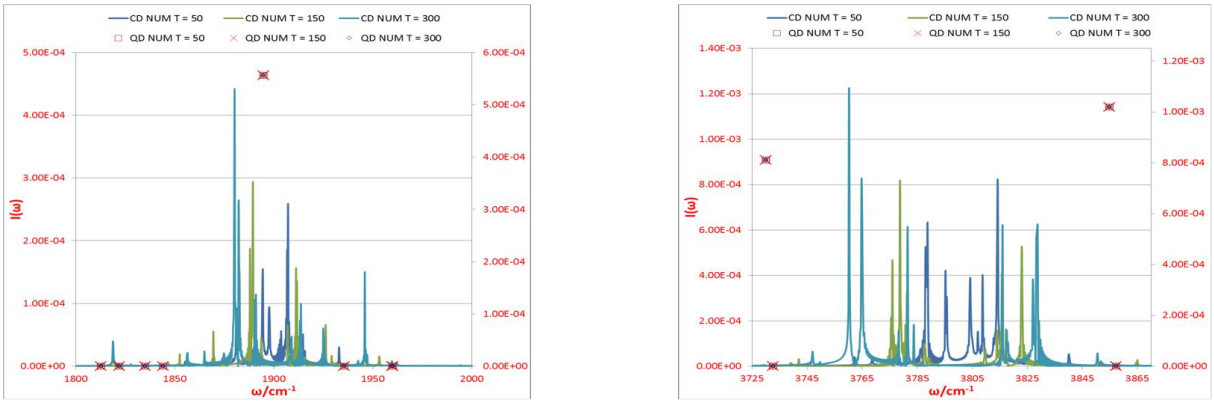

Figure 3. Temperature dependence of the Fermi-resonant coupled-oscillator spectrum at fixed coupling strength: (a) lower-frequency spectral region near 1900 cm^{-1} and (b) higher-frequency region near 3800 cm^{-1}.

Classical molecular-dynamics spectra at 50, 150, and 300 K are shown as solid curves; the corresponding quantum transitions are shown by symbols. Increasing temperature produces progressively greater structure in the classical spectra, whereas quantum transition frequencies remain comparatively stable and temperature primarily modifies state populations. Classical and quantum intensities use separate ordinates.

The classical spectra became progressively more complex as the temperature increased. Greater thermal energy increases the trajectory amplitudes and allows the system to explore more anharmonic regions of the potential-energy surface. Nonlinear interactions contribute additional dynamic frequencies, producing new peaks and fragmenting the spectral envelope. Thus, temperature not only expands the classical bands but also extends the frequency spectrum depicted by the Fourier-transformed motion.

The contrast may be expressed physically as follows: increasing temperature expands the phase-space region sampled by classical trajectories, whereas in the quantum description, it mainly redistributes populations among pre-existing discrete states. Although quantum spectra may develop temperature-dependent intensities or hot bands when excited states are populated, the temperature does not continuously alter the underlying eigenvalue differences of the quantum states. In contrast, the classical spectrum changes continuously with the amplitudes sampled on an anharmonic potential.

Consequently, thermal excitation amplifies the disparities caused by anharmonicity and coupling. This result is practically significant for condensed-phase spectra simulations, where finite temperature effects are unavoidable.

Classical MD can reproduce the principal experimental envelope while simultaneously generating weak temperature-dependent features without direct quantum correlations. Consequently, such bands should be assigned with caution.

3.4. Classical Description of Fermi Resonance

Fermi resonance provides a more demanding test because it results from anharmonic interactions between vibrational states that are nearly degenerate. The model contains modes of 3800 and 1900 cm^{-1}, such that the higher-frequency fundamental lies close to the overtone of the lower frequency mode. Figure 4.4 compares the quantum and classical spectra as the interaction changes from COUP0, representing the uncoupled system, to COUP1, representing weak coupling, and COUP2, representing strong coupling.

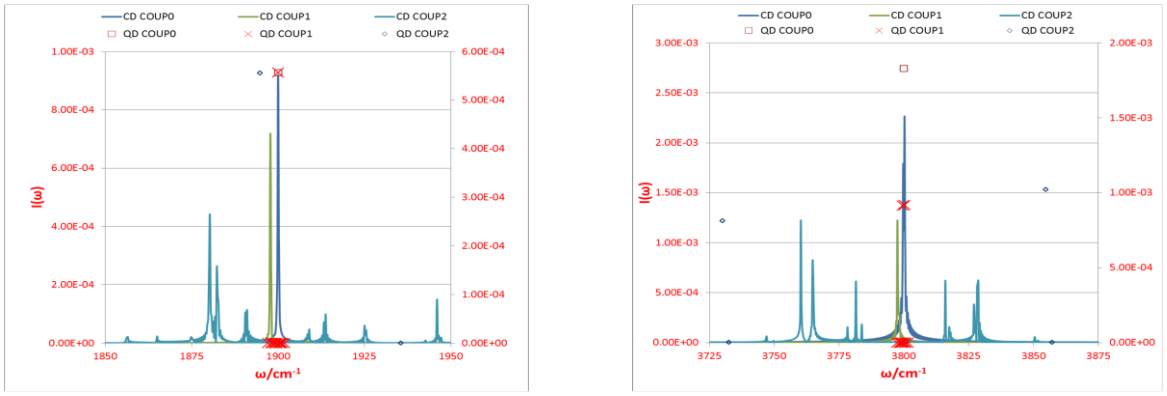

Figure 4. Evolution of Fermi resonance with increasing coupling strength at 300 K: (a) lower-frequency region near 1900 cm^{-1} and (b) higher-frequency region near 3800 cm^{-1}.

COUP0, COUP1, and COUP2 represent the uncoupled, weakly coupled, and strongly coupled systems, respectively. Solid curves denote classical molecular-dynamics spectra, whereas symbols denote quantum transitions. Both descriptions reproduce coupling-induced spectral splitting, but the strongly coupled classical spectrum contains a larger number of additional components. Classical and quantum intensities are displayed using separate ordinates.

Both approaches reproduce the principal signature of Fermi resonance. In the uncoupled system, the expected independent vibrational features were observed. Increasing the interaction separates the nearly degenerate features and produces a recognizable splitting pattern, indicating the mixing of interacting motions. Therefore, classical MD can detect the presence of vibrational coupling and reproduce the qualitative evolution of resonance.

The quantitative agreement deteriorated as the coupling strength increased. The quantum spectrum retained a relatively simple pattern containing a limited number of transitions. The classical spectrum developed a larger

number of components around the principal resonance frequencies and became particularly congested for COUP2. Therefore, strong anharmonic interactions enrich the set of nonlinear classical frequencies more rapidly than they increase the number of prominent quantum transitions in the system.

In the quantum description, Fermi resonance involves the mixing of specific discrete states, accompanied by level repulsion and the redistribution of the transition intensity. Classical trajectories can reproduce coupled motion and the associated frequency splitting; however, they do not represent the mixing between discrete eigenstates in the same manner. This distinction explains why the existence and evolution of the resonance were reproduced more successfully than its detailed structure.

Higher-order anharmonic motion and finite-time spectral processing may also contribute to this phenomenon. Therefore, it is preferable to describe them as additional classical spectral components consistent with higher-order vibrational interactions without assigning each peak to a specific transition.

Classical MD identifies Fermi coupling and predicts increasing splitting but overestimates the spectral complexity in the strongly coupled regime. Therefore, accurate transition positions, intensities, and resonance assignments require quantum treatment when the coupling is strong.

3.5. Domain of Validity of Classical Molecular Dynamics

The results show that the reliability of classical MD varies continuously with the quantum characteristics of vibration. It performs best for low-frequency modes with moderate anharmonicity when the objective is to reproduce the dominant band, overall spectral envelope, or qualitative trend. Under these conditions, the classical and quantum peak positions were similar, and the nonlinear dipole functions produced comparable general patterns.

The reliability decreases for high-frequency vibrations because the classical trajectories omit the discrete energy levels and zero-point motion. Electrical anharmonicity exposes this limitation by generating higher-order features, whose classical blue shifts increase rapidly with the spectral order. Elevated temperatures further increase the classical spectral complexity by expanding the anharmonic region sampled by the trajectories. Strong vibrational coupling presents the most demanding situation: classical MD reproduces the onset of Fermi splitting but generates more spectral components than the corresponding quantum calculations.

Therefore, the limitations arise from the combined influence of the high frequency, nonlinear dipole behavior, thermal excitation, and anharmonic coupling, rather than from a single factor. The effects of these factors are cumulative in nature. A high-frequency vibration with a nonlinear dipole function and strong coupling is expected to exhibit a substantially greater classical–quantum disagreement than a low-frequency, weakly anharmonic isolated mode.

Classical molecular dynamics (MD) is particularly suitable for investigating large molecular systems, low-frequency vibrational motions, environmental influences, qualitative band assignments, and overall spectral profiles, especially when computational efficiency is a major consideration. In contrast, an explicit quantum-mechanical treatment is generally required for the accurate description of high-frequency transitions, overtone intensities, strongly coupled vibrational states, and specific resonance interactions. Figure 4.5 illustrates this progressive shift from a largely classical description to a regime in which quantum effects become indispensable.

4. Implications for Molecular Dynamics Simulations of Real Systems

Despite relying on simplified Morse-potential representations, the present calculations provide a useful basis for understanding the vibrational spectra of liquids, biomolecular systems, polymers, and other condensed-phase materials. Classical molecular dynamics is well suited to these applications because it can describe thermal effects, conformational fluctuations, and interactions with the surrounding environment without excessive computational

expense. However, similarity between a calculated spectrum and its experimental counterpart should not be regarded as conclusive evidence that the associated quantum dynamics have been captured correctly. Inaccuracies in individual transition energies and intensities may remain hidden because of thermal broadening, averaging over different molecular environments, and limitations in experimental resolution. Consequently, classical simulations are most reliable for examining low-frequency vibrations, general spectral profiles, and qualitative structural variations. Greater caution is required for high-frequency stretching vibrations, overtones, strong anharmonicity, and Fermi resonance, for which quantum calculations are preferred. A practical strategy is to use classical dynamics for large-scale spectral screening and quantum methods for selected bands that require accurate assignment. When combined, these two methods offer a framework that is both efficient and physically dependable for real molecular systems in the gas phase.

5. Conclusions

This study examined the extent to which classical molecular dynamics can reproduce quantum vibrational spectra by employing both isolated and coupled Morse oscillators. The classical treatment successfully recovered the dominant spectral characteristics of low-frequency vibrations and provided a qualitative description of the effects associated with nonlinear dipole behaviour, temperature, and Fermi coupling. Its accuracy, however, decreased for high-frequency modes, higher-order transitions, increased temperatures, and strongly coupled vibrations. These limitations reflect the inability of classical trajectories to represent quantized vibrational energy levels, zero-point energy, and quantum-mechanical mixing between vibrational states. Nonlinear dipole functions and thermal excitation further increased the differences between the classical and quantum spectra. Strong vibrational coupling also generated additional components in the classical spectrum that were absent from the quantum results. Classical molecular dynamics is therefore most reliable for low-frequency motions, qualitative band assignments, and general spectral profiles. It is particularly useful for large molecular systems. Quantum calculations, however, are required for accurate high-frequency transitions, overtone intensities, and detailed resonance assignments. The two approaches should therefore be considered complementary tools in computational vibrational spectroscopy.

References

[1] E.B. Wilson Jr., J.C. Decius, P.C. Cross, Molecular Vibrations: The Theory of Infrared and Raman Vibrational Spectra, McGraw-Hill, New York, 1955.

[2] K. Nakamoto, Infrared and Raman Spectra of Inorganic and Coordination Compounds, Part B: Applications in Coordination, Organometallic, and Bioinorganic Chemistry, sixth ed., John Wiley & Sons, Hoboken, NJ, 2009.

[3] P.W. Atkins, R.S. Friedman, Molecular Quantum Mechanics, fifth ed., Oxford University Press, Oxford, 2010.

[4] M.P. Allen, D.J. Tildesley, Computer Simulation of Liquids, second ed., Oxford University Press, Oxford, 2017.

[5] P. Hamm, M.T. Zanni, Concepts and Methods of 2D Infrared Spectroscopy, Cambridge University Press, Cambridge, 2011.

[6] M. Born, R. Oppenheimer, On the quantum theory of molecules, in: H. Hettema (Ed.), Quantum Chemistry: Classic Scientific Papers, World Scientific, Singapore, 2000, pp. 1–24, https://doi.org/10.1142/9789812795762_0001.

[7] P.M. Morse, Diatomic molecules according to the wave mechanics. II. Vibrational levels, Phys. Rev. 34 (1929) 57–64, https://doi.org/10.1103/PhysRev.34.57.

[8] E. Fermi, Über den Ramaneffekt des Kohlendioxyds, Z. Phys. 71 (1931) 250–259, https://doi.org/10.1007/BF01341712.

[9] P.H. Berens, K.R. Wilson, Molecular dynamics and spectra. I. Diatomic rotation and vibration, J. Chem. Phys. 74 (1981) 4872–4882, https://doi.org/10.1063/1.441739.
[10] J.M. Bowman, The self-consistent-field approach to polyatomic vibrations, Acc. Chem. Res. 19 (1986) 202–208, https://doi.org/10.1021/ar00127a002.
[11] H.-D. Meyer, U. Manthe, L.S. Cederbaum, The multi-configurational time-dependent Hartree approach, Chem. Phys. Lett. 165 (1990) 73–78, https://doi.org/10.1016/0009-2614(90)87014-I.
[12] S. Carter, J.M. Bowman, N.C. Handy, Extensions and tests of "MULTIMODE": A code to obtain accurate vibration/rotation energies of many-mode molecules, Theor. Chem. Acc. 100 (1998) 191–198, https://doi.org/10.1007/s002140050379.
[13] M.H. Beck, A. Jäckle, G.A. Worth, H.-D. Meyer, The multiconfiguration time-dependent Hartree (MCTDH) method: A highly efficient algorithm for propagating wavepackets, Phys. Rep. 324 (2000) 1–105, https://doi.org/10.1016/S0370-1573(99)00047-2.
[14] V. Barone, Anharmonic vibrational properties by a fully automated second-order perturbative approach, J. Chem. Phys. 122 (2005) 014108, https://doi.org/10.1063/1.1824881.
[15] A.G. Császár, C. Fábri, T. Szidarovszky, E. Mátyus, T. Furtenbacher, G. Czakó, The fourth age of quantum chemistry: Molecules in motion, Phys. Chem. Chem. Phys. 14 (2012) 1085–1106, https://doi.org/10.1039/C1CP21830A.
[16] M. Thomas, M. Brehm, R. Fligg, P. Vöhringer, B. Kirchner, Computing vibrational spectra from ab initio molecular dynamics, Phys. Chem. Chem. Phys. 15 (2013) 6608–6622, https://doi.org/10.1039/C3CP44302G.
[17] J. Horníček, P. Kaprálová, P. Bouř, Simulations of vibrational spectra from classical trajectories: Calibration with ab initio force fields, J. Chem. Phys. 127 (2007) 084502, https://doi.org/10.1063/1.2756837.
[18] O. Marsalek, T.E. Markland, Quantum dynamics and spectroscopy of ab initio liquid water: The interplay of nuclear and electronic quantum effects, J. Phys. Chem. Lett. 8 (2017) 1545–1551, https://doi.org/10.1021/acs.jpclett.7b00391.
[19] E.L. Sibert III, Modeling vibrational anharmonicity in infrared spectra of high-frequency vibrations of polyatomic molecules, J. Chem. Phys. 150 (2019) 090901, https://doi.org/10.1063/1.5079626.
[20] E. Ditler, S. Luber, Vibrational spectroscopy by means of first-principles molecular dynamics simulations, WIREs Comput. Mol. Sci. 12 (2022) e1605, https://doi.org/10.1002/wcms.1605.
[21] E.L. Sibert III, Modeling anharmonic effects in the vibrational spectra of high-frequency modes, Annu. Rev. Phys. Chem. 74 (2023) 219–244, https://doi.org/10.1146/annurev-physchem-062422-021306.
[22] D.S. Tikhonov, Y.V. Vishnevskiy, Describing nuclear quantum effects in vibrational properties using molecular dynamics with Wigner sampling, Phys. Chem. Chem. Phys. 25 (2023) 18406–18423, https://doi.org/10.1039/D3CP01007D.
[23] Y. Zhang, Y. Wang, X. Xu, Z. Chen, Y. Yang, Vibrational spectra of highly anharmonic water clusters: Molecular dynamics and harmonic analysis revisited with constrained nuclear–electronic orbital methods, J. Chem. Theory Comput. 19 (2023) 9358–9368, https://doi.org/10.1021/acs.jctc.3c01037.
[24] S.C. Althorpe, Path integral simulations of condensed-phase vibrational spectroscopy, Annu. Rev. Phys. Chem. 75 (2024) 397–420, https://doi.org/10.1146/annurev-physchem-090722-124705.
[25] D.S. Tikhonov, PyRAMD scheme: A protocol for computing the infrared spectra of polyatomic molecules using ab initio molecular dynamics, Spectrosc. J. 2 (2024) 171–187, https://doi.org/10.3390/spectroscj2030012.
[26] H. Mitra, D. Sharma, T.K. Roy, Vibrational mode tailoring approach: An efficient route to compute anharmonic molecular vibrations of large molecules, Phys. Chem. Chem. Phys. 26 (2024) 29432–29448, https://doi.org/10.1039/D4CP02812K.

[27] T. Li, J. Huang, C. Li, D. Pan, Ab initio vibrational spectroscopy of water and aqueous solutions in a wide pressure–temperature range, WIREs Comput. Mol. Sci. 15 (2025) e70017, https://doi.org/10.1002/wcms.70017.

[28] V. Andreichev, S. Käser, E.L. Bocanegra, M. Salik, M.A. Johnson, M. Meuwly, Dynamics of protonated oxalate from machine-learned simulations and experiment: Infrared signatures, proton-transfer dynamics and tunnelling splittings, Phys. Chem. Chem. Phys. 27 (2025) 23288–23300, https://doi.org/10.1039/D5CP03085D.

[29] R. Conte, C. Aieta, M. Ceotto, Quantum vibrational spectroscopy with classical trajectories, Chem. Sci. 17 (2026) 3430–3448, https://doi.org/10.1039/D5SC09965J.

[30] G. Botti, G. Mandelli, Nuclear quantum effects and vibrational resonances in organic hydrates: Theoretical and experimental insights from DMSO monohydrate, Chem. Sci. 17 (2026) 7171–7177, https://doi.org/10.1039/D5SC08339G.